

Possible TCRM acquisition of the Kilauea 1960 lava, Hawaii: failure of the Thellier paleointensity determination inferred from equilibrium temperature of the Fe-Ti oxide

Yuhji Yamamoto*

Geological Survey of Japan, AIST, Tsukuba, Ibaraki 305-8567, Japan

(Received February 17, 2006; Revised April 14, 2006; Accepted April 15, 2006; Online published September 16, 2006)

Natural rock samples may not always be the ideal material for the Thellier-type method as they occasionally result in high paleointensities. The Kilauea 1960 lava, Hawaii, is one such example. Several previous studies have suggested that one of the possible causes for this undesirable behavior is an acquisition of thermochemical remanent magnetization (TCRM) during lava formation. In order to examine this possibility quantitatively, equilibrium temperatures of titanomagnetite grains, which are associated with samples previously subjected to Thellier experiments, are estimated by a Fe-Ti oxide geothermometer. The results show that two specimens from the rock magnetic group giving relatively ideal Thellier paleointensities have clustered equilibrium temperatures of about 800–900 and 700–800°C. In contrast, two swarmed temperatures around 300 and 700°C were observed for the specimen from a group yielding high paleointensities. Although these are semi-quantitative estimates, when the time scales of Fe-Ti interdiffusion and lava cooling are taken into consideration, the last specimen could have acquired the TCRM during its formation. For such specimens, simple calculation predicts that TCRM/TRM (thermoremanent magnetization) ratios could be 1.19–1.72 for the blocking temperature range of 400–480°C, assuming a grain-growth model. The extent of this overestimation (20–70%) is comparable to the magnitude of the observations. It is therefore suggested that attention be paid to titanomagnetite grains with well-developed ilmenite lamellae, as these could be potential sources of overestimations of Thellier paleointensities of up to a few tenths of percentage points.

Key words: Thermochemical remanent magnetization (TCRM), Thellier method, Hawaii, high temperature oxidation, geothermometer.

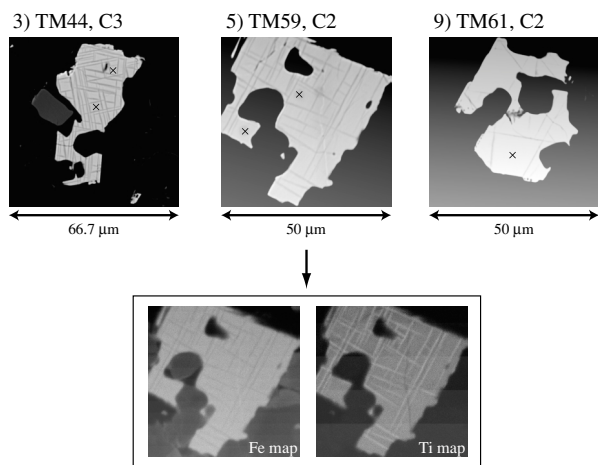
1. Introduction

The ability to make precise determinations of absolute paleointensities is an essential criterion for investigating the evolution of the geodynamo, as this in turn provides information on the Earth's core. To date, the Thellier-type method (e.g. Thellier and Thellier, 1959; Coe, 1967) has been the most frequently used method and the one considered to be the most reliable by many paleomagnetists (e.g. Valet, 2003). However, natural rock samples may not always be the ideal material for this method: evidence is accumulating which indicates that the Thellier-type method is not always robust for historical lava flows, resulting in systematic high paleointensities (e.g. Hill and Shaw, 2000; Calvo *et al.*, 2002; Yamamoto *et al.*, 2003; Mochizuki *et al.*, 2004; Oishi *et al.*, 2005). New protocols or strict criteria for obtaining reliable Thellier paleointensities have been proposed, and the outcomes obtained with these protocols appear to be successful (e.g. Biggin and Thomas, 2003; Chauvin *et al.*, 2005; Yu and Tauxe, 2005).

Independent of these improvements, it is important to investigate the cause of the high Thellier paleointensities. Several possibilities have been proposed: multi-domain (MD) or pseudo-single domain (PSD) effects (e.g. Levi, 1977; Kostrov and Prevôt, 1998; Calvo *et al.*, 2002; Xu and Dunlop, 2004), cooling-rate effect (e.g. Dodson and McClelland, 1980; Fox and Aitken, 1980; Tauxe, 2006), magnetic interaction between particles (e.g. Mankinen and Champion, 1993; Mochizuki *et al.*, 2004), among others. One possible cause which has been proposed is the acquisition of thermochemical remanent magnetization (TCRM), which is the magnetization acquired when slow cooling is accompanied by volume growth of a magnetic phase below its Curie temperature (Dunlop and Özdemir, 1997). Grommé *et al.* (1969) first pointed out that in some basaltic lavas the magnetic minerals may form through subsolidus reactions at temperatures well below their final Curie temperatures, resulting in a mixture of thermoremanent magnetization (TRM) and TCRM. Kellogg *et al.* (1970) subsequently concluded that paleointensity experiments could give reasonable values even if TCRM provided a considerable part of the natural remanent magnetization (NRM). However, McClelland (1996) numerically showed that grain-growth CRM (crystallization remanent magnetization) at high temperatures could result in an overestimation of the paleointensity.

*Now at: Geomagnetism Laboratory, The University of Liverpool, Liverpool L69 7ZE, UK.

(A) BEIs of titanomagnetite grains



(B) BEIs of titanohematite grains

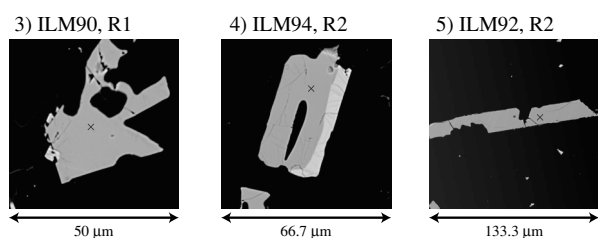
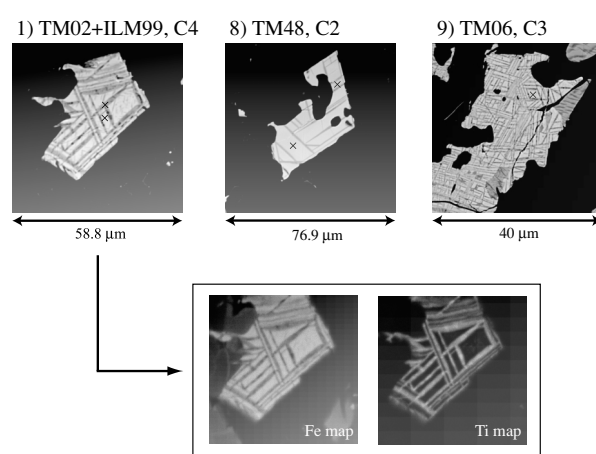


Fig. 1. Representative backscattered electron images (BEIs) of (A) titanomagnetite and (B) titanohematite grains of the specimen A-5. Crossed symbols are selected points for the quantitative analyses. The number indicated in upper left of each BEI corresponds to that in Table 1 (if there are two analyzed points in each BEI, averaged chemical compositions are indicated in the table). The Ti-rich component in the titanomagnetite (TM) or titanohematite (TH) phase and the identified oxidation index (C1–C7 or R1–R7 by Haggerty (1991)) are also shown. For the fifth TM grain in Table 1, element maps of Fe and Ti are displayed.

Yamamoto *et al.* (2003) obtained a number of high Thellier paleointensities from the Kilauea 1960 lava, Hawaii. Their samples showed different degrees of high temperature oxidation and, consequently, could be classified into rock magnetic groups of A, B, and C based on increasing levels of oxidation. The group B samples were characterized by an abundance of Ti-poor titanomagnetites (TMs) with well-developed ilmenite lamellae. Since these samples showed particularly high paleointensities, Yamamoto *et al.* (2003) suggested that the anomalous paleointensities could originate from the TCRM.

It is important to examine this hypothesis in a more quantitative fashion. One possible approach is to estimate the equilibrium temperature of iron-titanium (Fe-Ti) oxides using a geothermometer. A probable pre-condition for acquisition of the TCRM is if the temperature for a certain TM grain coexisting with exsolved ilmenite lamellae is below its Curie temperature. Although several types of Fe-Ti oxide geothermometers are available (e.g. Buddington and Lindsley, 1964; Ghiorso and Sack, 1991), that of Ghiorso (1997) is the only one incorporating a concept of magnetic ordering. For example, an equilibrium temperature for coexisting $\text{Fe}_{2.95}\text{Ti}_{0.05}\text{O}_4$ (TM05, 5 mol% of ulvöspinel) and $\text{Fe}_{1.04}\text{Ti}_{0.96}\text{O}_3$ (ILM96, 96 mol% of ilmenite) is 290°C

(A) BEIs of titanomagnetite grains



(B) BEIs of titanohematite grains

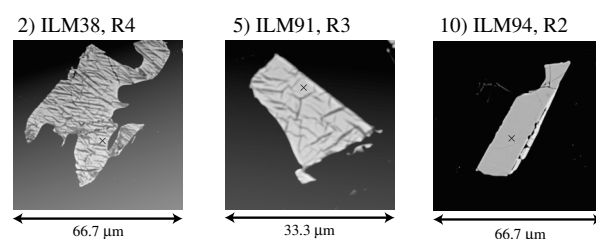


Fig. 2. Representative BEIs of (A) titanomagnetite and (B) titanohematite grains of the specimen B-6. The number indicated in upper left of each BEI corresponds to that in Table 2. For the first TM grain in Table 2, element maps of Fe and Ti are shown.

(Ghiorso, 1997), which is about 250°C lower than the Curie temperature of TM05 (estimated from a formula by Nagata (1962)), indicating a probable condition of the TCRM acquisition.

In this paper, I attempt to estimate the equilibrium temperatures of TM grains involved in the samples used in the paleointensity study by Yamamoto *et al.* (2003) (Kilauea 1960 lava, Hawaii). Based on the results, I discuss the relationship between the equilibrium and Curie temperatures of the samples. These estimations require that the chemical compositions of both TM hosts and coexisting ilmenite lamellae be determined and are undertaken by a combined approach of analyses by an electron probe micro-analyzer (EPMA) and measurements of magnetic susceptibilities at both low and high temperatures.

2. Samples

The samples subjected to the present analyses had been collected for the study of Yamamoto *et al.* (2003). They were drilled from an outcrop of the Kilauea 1960 lava, Hawaii, and were classified into three groups (A, B, and C) according to increasing high temperature oxidation states (C1–C3, C2–C4, and C4–C7; Haggerty (1991)). Haggerty (1991) defined the stages of high-temperature oxidation in TM and titanohematite (TH) grains as follows.

<Titanomagnetite grains>

C1: Optically homogeneous ulvöspinel-rich magnetite solid solutions (ss);

C2: Magnetite-enriched_{ss} with a small number of “ex-

Table 1. EPMA analytical results for the specimen A-5. Results are shown for the TM phase of 11 titanomagnetite grains (1–11) and the TH phase of nine titanohematite grains (1–9). As for the latter, average composition (Ave.) is also shown. Compositions of Fe₂O₃ and FeO are calculated from total Fe following Carmichael (1967). Molecular fractions of ulvöspinel or ilmenite in titanomagnetite or titanohematite (Ti-rich comp.) are determined by a procedure by Anderson (1968).

Titanomagnetite											
	1)	2)	3)	4)	5)	6)	7)	8)	9)	10)	11)
SiO ₂	0.18	0.20	0.16	0.21	0.19	0.19	0.22	0.22	0.19	0.16	0.24
TiO ₂	19.39	16.28	14.17	17.18	20.44	19.25	19.06	17.75	21.29	20.76	16.02
Al ₂ O ₃	1.65	2.24	2.24	1.59	1.78	1.55	1.66	1.86	1.75	1.92	2.12
MnO	0.26	0.27	0.26	0.32	0.25	0.29	0.28	0.31	0.21	0.30	0.29
MgO	1.23	0.83	0.58	0.80	1.22	1.20	0.97	0.90	1.37	1.21	0.80
CaO	0.03	0.20	0.08	0.14	0.09	0.12	0.05	0.25	0.13	0.12	0.35
Cr ₂ O ₃	0.09	0.09	0.10	0.06	0.07	0.03	0.06	0.03	0.01	0.03	0.09
FeO	69.65	70.45	73.81	73.12	70.90	72.41	71.51	72.22	69.60	71.03	74.03
Total	92.48	90.54	91.39	93.40	94.94	95.04	93.81	93.53	94.56	95.54	93.93
Fe ₂ O ₃	26.39	30.44	35.34	31.48	25.87	28.74	27.83	30.13	24.04	25.58	33.53
FeO	45.91	43.05	42.00	44.79	47.62	46.54	46.47	45.11	47.97	48.01	43.86
Total	95.12	93.59	94.93	96.56	97.53	97.92	96.60	96.55	96.97	98.11	97.28
Ti-rich comp.	0.57	0.52	0.44	0.52	0.59	0.55	0.55	0.54	0.61	0.59	0.49

Titanohematite										
	1)	2)	3)	4)	5)	6)	7)	8)	9)	Ave.
SiO ₂	0.09	0.11	0.12	0.08	0.15	0.16	0.09	0.14	0.13	0.12
TiO ₂	47.32	46.93	46.86	49.00	48.26	48.82	49.17	49.28	50.71	48.48
Al ₂ O ₃	0.15	0.13	0.21	0.16	0.16	0.19	0.18	0.17	0.12	0.16
MnO	0.26	0.35	0.32	0.33	0.33	0.40	0.24	0.42	0.42	0.34
MgO	1.47	1.81	1.53	1.97	1.51	1.62	1.45	1.50	2.13	1.66
CaO	0.10	0.26	0.07	0.09	0.09	0.19	0.10	0.12	0.07	0.12
Cr ₂ O ₃	0.06	0.05	0.05	0.00	0.00	0.04	0.01	0.07	0.04	0.04
FeO	47.15	47.04	47.62	45.77	47.66	46.95	47.35	47.12	46.45	47.01
Total	96.59	96.66	96.78	97.41	98.15	98.36	98.59	98.81	100.08	97.94
Fe ₂ O ₃	8.32	9.55	9.41	6.19	7.99	7.09	6.64	6.52	5.56	7.47
FeO	39.66	38.44	39.15	40.20	40.46	40.57	41.38	41.26	41.45	40.29
Total	97.42	97.62	97.72	98.03	98.95	99.07	99.26	99.46	100.63	98.69
Ti-rich comp.	0.91	0.90	0.90	0.94	0.92	0.93	0.93	0.93	0.94	0.92

solved” ilmenite lamellae parallel to 111 of the host;

C3: Ti-poor titanomagnetite_{ss} with densely crowded “exsolved” ilmenite lamellae parallel to 111;

C4: The first sign of additional oxidation; optically, an indistinct mottling of the ilmenomagnetite intergrowth is observed;

C5: Rutile + titanohematite develop extensively within the “exsolved” metailmenite lamellae;

C6: Incipient formation of pseudobrookite_{ss} (Psb_{ss}) from rutile + titanohematite;

C7: Assemblage of Psb_{ss} + hematite_{ss}; most advanced stage of oxidation of original spinels.

<Titanohematite grains>

R1: Homogenous ilmenite;

R2: Onset of fine wisp-like sigmoidal lenses of ferrian rutile;

R3: The lenses become thicker and more abundant;

R4: Marked reflectivity in both the host and the lamellar components;

R5: Extensive development of rutile and titanohematite;

R6: Development of Psb_{ss} from the R5 assemblage;

R7: Predominance of pseudobrookite.

In Yamamoto *et al.* (2003), the Coe’s version of the Thellier method (Thellier and Thellier, 1959; Coe, 1967) was applied to 19 core samples. These paleointensities (averages and standard deviations) resulted in $41.9 \pm 4.2 \mu\text{T}$ ($n = 4$), $56.0 \pm 7.6 \mu\text{T}$ ($n = 9$), and $40.6 \pm 3.2 \mu\text{T}$ ($n = 4$) for the A, B, and C groups, respectively (Yamamoto *et al.*, 2003). All of the values exceeded the expected value ($36.2 \mu\text{T}$), and the group B samples gave particularly high Thellier paleointensities. The analyses reported here were mainly conducted on a representative sample from each group. Unheated parts of samples A-5, B-6, and C-1 were cut into several pieces and subjected to the EPMA analyses or the susceptibility measurements.

3. EPMA Analyses

Sliced pieces from each sample (A-5, B-6, and C-1) were impregnated with epoxy and subsequently polished to mirror gloss. These were then observed and analyzed by a JEOL-JXA-8800 electron microprobe at the Tokyo Institute of Technology, Japan. TM or TH grains some tens of micrometers in size were searched out for observational and analytical purposes, and backscattered electron images

Table 2. EPMA analytical results for the specimen B-6. Results are shown for the coexisting TM and TH phases of six titanomagnetite grains (1–6), the TM phase of seven titanomagnetite grains (7–13), and the TH phase of 16 titanohematite grains (1–16).

	Titanomagnetite + Titanohematite											
	1) TM	TH	2) TM	TH	3) TM	TH	4) TM	TH	5) TM	TH	6) TM	TH
SiO ₂	0.17	0.19	0.17	0.20	0.15	0.18	0.12	0.18	0.13	0.12	0.17	0.23
TiO ₂	1.51	48.76	2.58	29.42	1.71	45.62	1.25	32.89	14.40	48.74	8.15	45.47
Al ₂ O ₃	1.01	0.44	4.32	1.27	2.98	0.37	1.54	2.08	1.83	0.05	2.85	0.27
MnO	0.16	0.34	0.03	0.19	0.08	0.48	0.99	0.32	0.26	0.44	0.05	0.35
MgO	0.73	1.16	1.48	0.82	0.84	1.48	1.57	1.51	0.61	1.55	0.54	1.41
CaO	0.05	0.06	0.15	0.25	0.13	0.33	0.05	0.14	0.14	0.25	0.11	0.32
Cr ₂ O ₃	0.08	0.11	0.08	0.09	0.10	0.05	0.06	0.02	0.07	0.01	0.12	0.00
FeO	85.78	41.91	79.79	57.75	82.15	44.78	84.48	53.72	74.86	45.35	78.48	45.28
Total	89.48	92.95	88.59	89.99	88.13	93.28	90.05	90.87	92.29	96.51	90.47	93.33
Fe ₂ O ₃	61.82	0.34	55.20	36.70	58.03	7.85	62.76	30.14	36.19	5.43	46.30	8.19
FeO	30.15	41.61	30.12	24.73	29.93	37.71	28.01	26.60	42.29	40.47	36.82	37.90
Total	95.67	92.98	94.12	93.67	93.95	94.07	96.34	93.88	95.92	97.05	95.11	94.15
Ti-rich comp.	0.02	1.00	0.09	0.60	0.05	0.92	0.04	0.66	0.44	0.95	0.26	0.91

	Titanomagnetite							Titanohematite				
	7)	8)	9)	10)	11)	12)	13)	1)	2)	3)	4)	5)
SiO ₂	0.17	0.17	0.14	0.18	0.12	0.15	0.17	0.08	0.11	0.13	0.08	0.12
TiO ₂	1.96	15.16	1.95	10.71	1.09	16.05	8.15	46.21	23.15	39.56	45.02	46.88
Al ₂ O ₃	3.48	1.98	3.01	2.13	3.38	1.80	2.85	0.10	0.18	0.15	0.15	0.12
MnO	0.09	0.20	0.22	0.31	1.31	0.26	0.05	0.53	0.59	0.67	0.90	0.62
MgO	0.81	0.65	1.38	0.47	2.57	0.81	0.54	2.28	3.11	3.06	3.72	2.13
CaO	0.11	0.13	0.00	0.03	0.14	0.20	0.11	0.12	0.05	0.25	0.20	0.11
Cr ₂ O ₃	0.10	0.08	0.08	0.10	0.06	0.11	0.12	0.06	0.01	0.07	0.01	0.05
FeO	82.58	71.95	83.55	76.95	80.10	73.16	78.48	46.12	62.70	50.12	44.05	45.37
Total	89.29	90.31	90.32	90.87	88.77	92.54	90.47	95.49	89.90	93.99	94.13	95.41
Fe ₂ O ₃	57.67	32.88	59.46	42.14	60.40	33.02	46.30	10.23	53.28	23.15	12.51	8.48
FeO	30.69	42.37	30.05	39.03	25.75	43.45	36.82	36.92	14.76	29.29	32.80	37.74
Total	95.07	93.61	96.28	95.10	94.82	95.84	95.11	96.52	95.24	96.31	95.38	96.26
Ti-rich comp.	0.06	0.48	0.06	0.33	0.03	0.49	0.26	0.89	0.38	0.74	0.86	0.91

	Titanohematite										
	6)	7)	8)	9)	10)	11)	12)	13)	14)	15)	16)
SiO ₂	0.19	0.09	0.11	0.08	0.12	0.21	0.08	0.10	0.06	0.11	0.10
TiO ₂	1.64	20.41	42.08	48.11	48.94	0.51	47.11	47.90	49.43	44.83	49.27
Al ₂ O ₃	0.06	0.16	0.17	0.12	0.13	0.13	0.06	0.14	0.08	0.15	0.12
MnO	0.02	0.55	0.42	0.22	0.38	0.00	0.86	0.34	0.56	0.58	0.41
MgO	0.13	2.21	2.53	1.59	1.77	0.07	3.48	1.71	2.28	2.63	1.88
CaO	0.12	0.09	0.19	0.12	0.09	0.05	0.08	0.16	0.11	0.16	0.08
Cr ₂ O ₃	0.00	0.00	0.03	0.01	0.03	0.03	0.08	0.00	0.04	0.06	0.10
FeO	84.30	65.88	49.07	46.79	45.25	85.74	44.42	46.03	44.76	44.77	45.96
Total	86.46	89.37	94.60	97.04	96.71	86.74	96.17	96.36	97.32	93.29	97.91
Fe ₂ O ₃	92.25	57.80	18.07	7.35	5.27	94.70	10.13	7.11	5.55	10.87	5.98
FeO	1.29	13.87	32.81	40.17	40.51	0.52	35.31	39.63	39.77	34.99	40.57
Total	95.70	95.16	96.41	97.78	97.24	96.23	97.19	97.07	97.87	94.38	98.51
Ti-rich comp.	0.03	0.35	0.80	0.93	0.94	0.01	0.89	0.93	0.94	0.88	0.94

(BEIs) were captured. Several points were selected in each grain and these were subjected to analyses of chemical composition. Quantitative analyses were performed using a WDS (wavelength dispersive X-ray spectrometer) with a focused beam (15 kV accelerating voltage and 12 nA cur-

rent), applying the ZAF correction method. The spot size of the beam is approximately 2–3 μm (analyses were made on areas larger than this spot size, the intra-texture of which appear to be homogeneous in BEIs). Counting time for Si, Ti, Al, Mg, Ca, Fe was set to be 20 s while that for

Mn and Cr was 30 s. Fe_2O_3 and FeO constituents were calculated from total Fe following Carmichael (1967), assuming stoichiometry of TM or TH phases. The molecular fractions of ulvöspinel and ilmenite were determined by a procedure developed by Anderson (1968). These computations were processed using ILMAT (Lepage, 2003). In subsequent sections of this article the chemical compositions of TM and TH solid solutions are expressed as TM_x ($\text{Fe}_{3-0.01x}\text{-Ti}_{0.01x}\text{-O}_4$) and ILMy ($\text{Fe}_{2-0.01y}\text{-Ti}_{0.01y}\text{-O}_3$), respectively. Although some of the assumptions used in Carmichael (1967) have been called into question in more recent studies (e.g. Stormer, 1983), the recalculations reported in this article did not result in significant differences in Fe_2O_3 compositions.

Eleven TM and nine TH grains were observed on the A-5 slice. Representative BEIs are shown in Fig. 1. All of the TM grains showed low-grade high temperature oxidation (C2–C3), which is visually recognizable from the element maps of Fe and Ti for a C2-class grain (Fig. 1, A5). The compositions of the hosts corresponded to TM44–TM61 (Table 1), while associated ilmenite lamellae were too narrow to be analyzed by the focused beam. The TH grains also exhibited low-grade high temperature oxidation (R1–R2), the compositions of which were determined to be ILM90–ILM94 (Table 1).

Observations were made on 13 TM and 16 TH grains of the B-6 slice. High-temperature oxidation states were intermediate in degree, typically C2–C4 and R1–R4. Representative BEIs and element maps of Fe and Ti are shown in Fig. 2. Quantitative analyses revealed that the compositions of the TM hosts ranged between TM02 and TM49, although about one-half of these resulted in TM02–TM09. The widths of the exsolved ilmenite lamellae of six of the 13 TM grains appeared to be large, and their compositions were determined to be ILM91–ILM100, with the exception of two grains. For the TH grains, 12 grains resulted in compositions of ILM74–ILM94, with the remainder showing more oxidized compositions. These analytical results are summarized in Table 2.

Both seven TM and TH grains were observed for the slice of C-1. Although there are many TM and TH grains with C6–C7 and R6–R7 oxidation, these were excluded from the present analysis because the pseudobrookite phase (generally involved in C6–C7 TM and R6–R7 TH grains) does not contribute to the Fe-Ti oxide geothermometry. All of the TM grains observed showed a sandwich-type high-temperature oxidation: large TM hosts associated with broad ilmenite lamellae (Fig. 3A). The compositions of the hosts and the lamellae were determined to be TM10–TM16 and ILM53–ILM73, respectively (Table 3). Element maps of Fe and Ti indicate that the host is almost free of Ti (Fig. 3A, 2). It is difficult to simply classify the oxidation indices of these grains. However, they could be categorized as a C4 oxidation state if the lamellae compositions were to be taken into account (in a mid-course of hematization). The TH grains exhibited two groups of oxidations: R1–R2 for three grains and R5–R7 for four grains. The chemical compositions are ILM44–ILM96 (Table 3).

The quality of the analytical results presented here is not actually that good because they show relatively low totals.

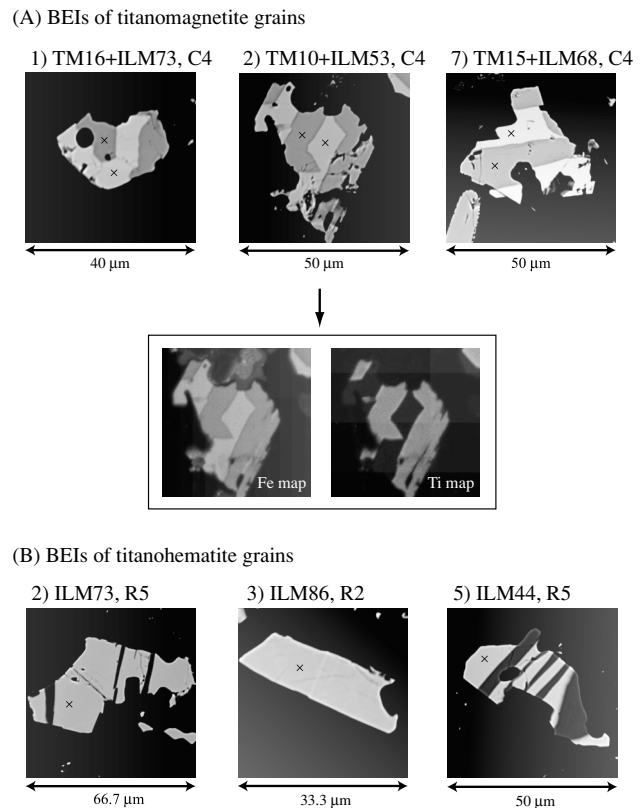


Fig. 3. Representative BEIs of (A) titanomagnetite and (B) titanohematite grains of the specimen C-1. The number indicated in upper left of each BEI corresponds to that in Table 3. For the second TM grain in Table 3, element maps of Fe and Ti are shown.

Even after redistributing iron as Fe^{3+} and Fe^{2+} , the total resulted in 93.6–98.1% and 93.0–100.6% for the TM and TH phase, respectively (Tables 1–3). There are two possible explanations for this. One is a moderate stability of the WDS equipment at the time of the analyses. A once-a-day quantitative analysis was performed on a laboratory standard sample (hornblende) in the present study. A series of results is listed in Table 4. While an average of five measurements almost corresponds to a reference value (which is determined from a wet analysis), there is a standard deviation (1σ) of 1.4% in a total value, which means that there is approximately a 3% uncertainty (2σ) in the present analytical results. Recalculations of iron can further propagate this error, possibly yielding the low total. The second explanation is that dehydration of the slices might be insufficient at a sample preparation stage. In this case, a small amount of H_2O may remain on the surface of the slices. The samples contained a very small proportion of H_2O (few percentage), which could cause the low total. The extent of the uncertainties could produce approximately a 1 and 2 mol% error in the calculation of ulvöspinel and ilmenite content in the TM and TH solid solutions, respectively. However, if the extent of these errors is taken into account, semi-quantitative discussions using the present results would seem to be possible.

The experimentally determined compositions of the TM and the TH grains are illustrated in $\text{FeO-TiO}_2\text{-Fe}_2\text{O}_3$ ternary diagrams (Fig. 4). Closed symbols indicate the composi-

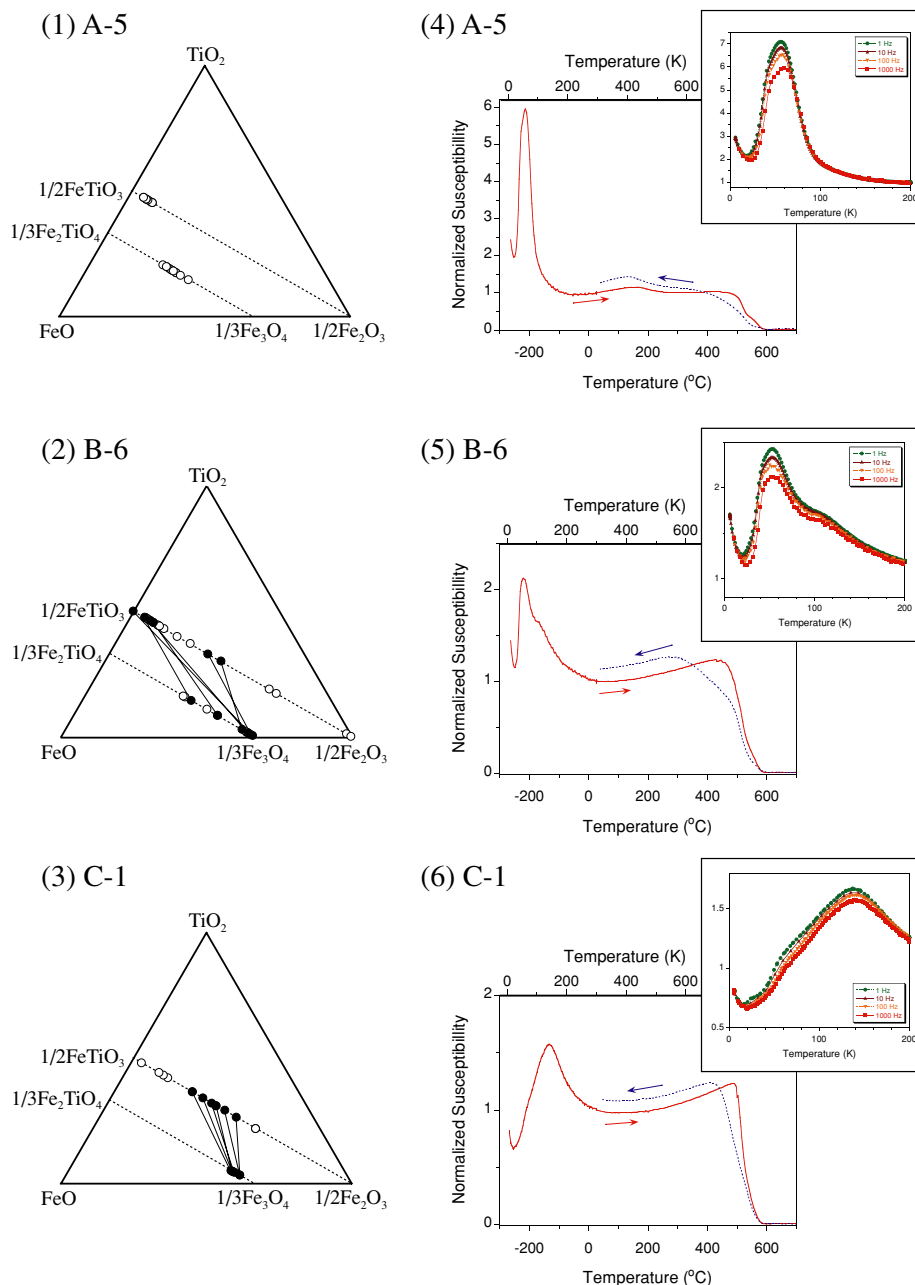


Fig. 4. (1–3) FeO-TiO₂ - Fe₂O₃ ternary diagrams of the specimens A-5, B-6, and C-1. They illustrate the chemical compositions of the TM and the TH grains determined by the EPMA analyses. Filled (open) circles are the analytical results of the host TM and lamellar TH phases (discrete TM and TH phases). (4–6) Magnetic susceptibility curves of the specimens A-5, B-6, and C-1. The curves are composed of the results of low-temperature and high-temperature runs. Both are normalized by susceptibility values at room temperature. Solid (dashed) lines in each lower left figure represent heating (cooling) curves in the high-temperature runs. Note that the low-temperature measurements were conducted with variable frequencies of 1, 10, 100 and 1000 Hz, and those at 1000 Hz are only indicated with the high-temperature results.

tions of both the TM host and the lamellar TH phase, while the open symbols show those of other phases. It is obvious that high-temperature oxidation progresses in the order of A-5, B-6, and C-1 because the symbols in the ternary diagrams move towards the lower right region in this order. This conclusion is the same as that drawn by Yamamoto *et al.* (2003).

4. Low- and High-Temperature Magnetic Susceptibilities

For a temperature range of 30 to 700°C, low-field susceptibilities were measured for powdered fractions from sam-

ples of A-5, B-6, and C-1 using a KLY-4S Kappabridge with a CS-3 furnace apparatus (AGICO). The measurements were performed in an argon gas flow with a constant field of 300 A/m (~ 4 Oe) and an operating frequency of 875 Hz. For low temperatures, in-phase AC susceptibilities (χ') were measured for small fragments (~ 10 mg) of each sample using a low-temperature SQUID susceptometer (Quantum Design MPMS-XL5). The measurements were carried out in a constant 80 A/m (1 Oe) field with variable frequencies (1, 10, 100, and 1000 Hz) over a temperature range of 6–300 K, sometimes 10–300 K. All of the experiments were carried out at the Geological Survey of Japan, AIST,

Table 3. EPMA analytical results for the specimen C-1. Results are shown for the coexisting TM and TH phases of seven titanomagnetite grains (1–7) and the TH phase of seven titanohematite grains (1–7).

	Titanomagnetite + Titanohematite											
	1) TM	TH	2) TM	TH	3) TM	TH	4) TM	TH	5) TM	TH	6) TM	TH
SiO ₂	0.21	2.68	0.14	0.11	0.16	0.11	0.18	0.10	0.20	0.12	0.19	0.12
TiO ₂	4.98	37.71	3.20	28.43	4.85	33.24	3.25	30.64	4.42	34.53	4.13	36.22
Al ₂ O ₃	3.27	0.47	3.86	0.54	3.22	0.48	3.38	0.45	3.08	0.36	3.30	0.36
MnO	0.20	0.27	0.27	0.18	0.20	0.21	0.17	0.18	0.22	0.21	0.23	0.30
MgO	1.46	2.64	1.73	2.02	1.42	2.06	1.33	2.14	1.58	2.64	1.56	2.87
CaO	0.17	0.29	0.04	0.09	0.09	0.08	0.09	0.11	0.16	0.18	0.13	0.09
Cr ₂ O ₃	0.08	0.05	0.09	0.09	0.08	0.05	0.16	0.07	0.13	0.04	0.08	0.06
FeO	79.80	50.49	81.72	59.85	80.15	58.43	82.13	58.14	81.34	55.76	80.17	55.31
Total	90.16	94.60	91.04	91.31	90.16	94.66	90.69	91.83	91.14	93.84	89.80	95.32
Fe ₂ O ₃	52.62	20.80	56.51	42.28	53.04	36.00	56.34	38.44	54.76	33.00	54.16	31.25
FeO	32.45	31.77	30.88	21.81	32.42	26.04	31.44	23.55	32.06	26.06	31.44	27.19
Total	95.43	96.69	96.70	95.55	95.48	98.27	96.33	95.68	96.62	97.14	95.22	98.45
Ti-rich comp.	0.16	0.73	0.10	0.53	0.15	0.62	0.10	0.58	0.14	0.64	0.13	0.66

	Titanohematite									
	7) TM	TH	1)	2)	3)	4)	5)	6)	7)	
SiO ₂	0.32	0.34	0.12	0.12	0.14	0.11	0.26	0.35	0.27	
TiO ₂	4.91	37.22	45.39	40.01	46.55	46.65	26.11	33.03	48.02	
Al ₂ O ₃	3.04	0.35	0.23	0.29	0.30	0.29	0.50	0.54	0.50	
MnO	0.23	0.28	0.38	0.45	0.39	0.35	0.43	0.27	0.31	
MgO	1.56	2.83	2.94	4.15	3.74	3.79	3.46	2.64	3.32	
CaO	0.07	0.08	0.01	0.07	0.24	0.15	0.25	0.12	0.22	
Cr ₂ O ₃	0.10	0.06	0.08	0.04	0.00	0.04	0.08	0.05	0.03	
FeO	82.08	54.28	48.43	49.30	46.66	44.32	60.36	55.40	40.44	
Total	92.31	95.44	97.59	94.43	98.02	95.69	91.44	92.39	93.10	
Fe ₂ O ₃	54.38	28.70	14.55	23.45	13.31	10.58	48.33	33.80	3.80	
FeO	33.16	28.45	35.34	28.19	34.69	34.80	16.87	24.99	37.02	
Total	97.76	98.31	99.05	96.78	99.35	96.75	96.28	95.78	93.49	
Ti-rich comp.	0.15	0.68	0.84	0.73	0.86	0.88	0.44	0.62	0.96	

and the results are shown in Fig. 4. In the figure, the susceptibilities are normalized by the room temperature values. Although results of the high-temperature runs displayed slight irreversible thermomagnetic curves (Fig. 4 (4)–(6)), these curves are considered to result from the reducing atmosphere (argon gas flow), and even more reversible curves would be obtained if the measurements were done in the air. In fact, most of the present samples showed positive pTRM checks up to about 500–600°C in the previous Thellier experiment conducted in the air (Yamamoto *et al.*, 2003).

The result of A-5 (Fig. 4 (4)) showed a sharp peak at 60 K, a bump at 160°C, and two phases of decrease at ~500°C and 550°C, respectively. The first peak is probably due to an emergence of a magnetic phase transition that occurred in the Ti-rich TH phase. This is because the Néel temperature of the ilmenite (end-member of TH phase) is 55 K (Ishikawa and Akimoto, 1985), and the present peak appears to be analogous to a temperature-dependent variation in a weak field magnetization of ILM90 (Fig. 5, modified from Ishikawa *et al.* (1985)). In fact, the EPMA analyses clearly demonstrated that the TH phase of A-5 corresponds to ILM90–94. The bump at ~160°C seems to originate from the TM phase. The EPMA analyses confirmed that there are

TM grains with the composition of TM44–TM61 in A-5. According to Nagata (1962), the Curie temperatures of this phase are 138–261°C, which are capable of explaining the bump. The remaining decrease at 500°C and 550°C cannot be explained by the EPMA results, but they may come from Ti-poor TM grains that are too tiny to be analyzed by the EPMA (smaller than 2–3 μm, the spot size of the beam).

In the susceptibility curve of B-6 (Fig. 4(5)), there are two peaks at ~55 K and ~450°C, and a minor inflection point at ~110 K. Similar to the above interpretation, these peaks could be explained by Ti-rich TH and Ti-poor TM phases. In the EPMA analyses, the TM grains with the TM02–TM09 composition were mainly recognized in B-6. Although the corresponding Curie temperatures of 515–566°C are higher than 450°C, they are within an interval of steep decline in susceptibility that continues from 450°C. Because there are slightly Ti-rich TM grains (Table 2), the peak at ~450°C can be accounted for by the Ti-poor TM grains. There are also TH grains of ILM74–ILM94 in B-6 and, compared with A-5, B-6 is slightly richer in Ti content. Thus, the peak at ~55 K is suppressed and extends towards the higher temperature. The inflection point at ~110 K can be explained by two possible factors. One is the relatively

Table 4. EPMA analytical results for the laboratory standard sample. Once-a-day measurements were performed five times, and their average and standard deviation is shown with a reference value which is previously determined by a wet analysis. Note that the sample contains a few percent of H₂O.

	Hornblende							
	02/19	03/08	03/11	03/19	03/22	ave.	stdev.	wet
SiO ₂	38.10	40.31	40.23	39.48	39.42	39.51	0.89	40.4
TiO ₂	5.78	5.67	5.56	5.71	5.65	5.68	0.08	5.5
Al ₂ O ₃	13.65	14.19	13.96	14.21	14.01	14.00	0.23	14.6
MnO	0.13	0.11	0.12	0.21	0.08	0.13	0.05	—
MgO	11.86	11.72	11.61	11.45	11.78	11.68	0.16	11.7
CaO	9.83	10.05	9.86	9.59	9.70	9.81	0.17	9.4
Cr ₂ O ₃	0.01	—	0.00	0.00	0.00	0.00	0.00	0.0
FeO	11.45	11.50	11.50	11.77	11.00	11.44	0.28	11.8
Na ₂ O	2.84	—	—	—	—	—	—	2.9
K ₂ O	1.64	—	—	—	—	—	—	1.5
Total	95.29	93.56	92.85	92.42	91.65	93.15	1.38	97.8

Ti-rich TH phase (approx. ILM85), which could produce a susceptibility peak around 110 K, if Fig. 5 were to be taken into consideration. The other is the Verwey transition, which is a phase transition from cubic to monoclinic symmetry (Verwey, 1939). This transition occurs at about 120 K for Ti-free TM (TM0), and the temperature decreases with an increase in the number of Ti substitutions (Dunlop and Özdemir, 1997). The existence of the TM phase of TM02-09 composition suggests that the Verwey transition is also the possible source of the inflection at ~110 K.

For the susceptibility curve of C-1 (Fig. 4 (6)), two peaks at ~140 K and ~500°C and a minor inflection point at ~60 K are recognized. Although the lamellar TH phase of ILM53–ILM73 (identified in the EPMA analyses, Table 3) probably results in a peak higher than 140 K, the TH grains of ILM73–ILM96 are possibly also responsible for the peak at ~140 K. The peak at ~500°C can be elucidated by the TM phase: the main TM phase of C-1 was identified as TM10–TM16 in the EPMA analyses and the corresponding Curie temperatures are 464–508°C. This phase may also accompany the Verwey transition, but there is not a clear peak around 110 K. This latter peak is probably overwhelmed by that at ~140 K. As for the inflection point at ~60 K, it is possible that some Ti-rich TH phase (e.g. the ILM96 grain; Table 3) survived the high-temperature oxidation and produced the inflection.

In summary, the low-temperature susceptibility curves imply the existence of the phases of approximately ILM90 for A-5, approximately ILM90 and approximately TM10 for B-6, and approximately ILM80 and approximately TM10 for C-1. The high-temperature curves suggest the phases of approximately TM60 and approximately TM10 in A-5, and approximately TM10 in both B-6 and C-1. Note that these compositions are semi-quantitatively approximated values.

5. Estimate of the Equilibrium Temperatures

In the EPMA analyses, chemical compositions of both host TM and lamellar TH phases could be determined for six and seven TM grains of B-6 and C-1, respectively. In

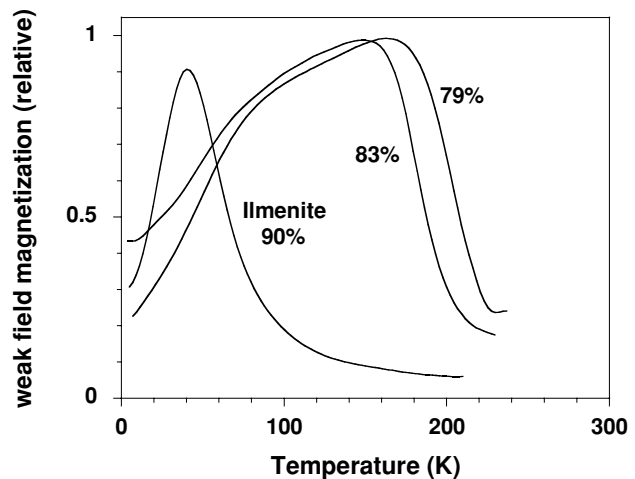


Fig. 5. Temperature-dependent variations in weak field magnetizations of ILM90, 83, and 79 (modified from Ishikawa *et al.* (1985)).

contrast, the quantitative analyses were successful only in determining host TM compositions for 11 TM grains of A-5 and seven TM grains of B-6. Applications of the Fe-Ti oxide geothermometer are straightforward for the former case but not for the latter. To estimate equilibrium temperatures of all of these TM grains, a rock magnetic approach was adopted to evaluate the compositions of the lamellar TH phase in the latter case.

The low-temperature susceptibility measurements suggest that the main TH phase of A-5 is approximately ILM90; in addition, there are no obvious peaks related to the other TH phase. It is possible to assume that the composition of the lamellar TH phase of A-5 is close to approximately ILM90, or more precisely, to an averaged composition of the discrete TH grains. This assumption is probably justified to some extent because the low-temperature susceptibility curves did not show significant frequency dependence (Fig. 4), thereby implying that the chemical compositions are not so variable among the TH phase of different domain sizes (from discrete grains to narrow lamellae). The result is ILM92 if the average composition is calculated from the analytical results of all nine TH grains (Table 1). This composition also seems to represent the undetermined lamellar TH phase in B-6 because both susceptibility curves of A-5 and B-6 commonly have the peaks at ~60 K (Fig. 4).

Based on these data, equilibrium temperatures are estimated for the observed TM grains using the Fe-Ti oxide geothermometer of Ghiorso (1997). The results are presented in Fig. 6 together with the Curie temperatures of titanomagnetites (Nagata, 1962). Figure 6 clearly shows that about one half of the TM grains in B-6 have equilibrium temperatures lower than the corresponding Curie temperatures. Most of these cluster around 300°C. Conversely, all TM grains of A-5 and C-1 have equilibrium temperatures higher than their Curie temperatures, with most concentrated around 800–900°C (A-5) and 700–800°C (C-1). These results suggest that the specimen of B-6 could acquire not only TRM but also TCRM during its formation.

These estimates seem to represent equilibrium temperatures of each group. To clarify this supposition, almost all of

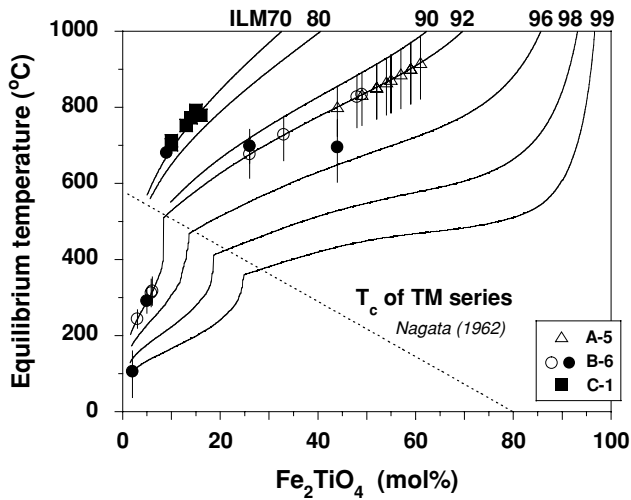


Fig. 6. Equilibrium temperatures estimated for the TM grains of the specimens A-5 (triangles), B-6 (circles), and C-1 (squares), using the Fe-Ti oxide geothermometer by Ghiorso (1997). Filled (open) symbols are the direct analytical results by EPMA (indirect results by both EPMA and susceptibility measurements). They are associated with error bars assuming the uncertainties of 2 mol% in ilmenite content in TH solid solutions. Solid lines represent iso-compositions of ILM70, 80, 90, 92, 96, 98 and 99, whereas a dashed line indicates the Curie temperature (T_c) of titanomagnetites (Nagata, 1962).

the samples were subjected to susceptibility measurements at high and low temperatures. Figure 7 shows the resultant susceptibility curves. Although three curves of group B samples appear to be analogous to those of group A, other curves show fairly consistent behavior within the group. This result suggests that the present analytical results of A-5, B-6, and C-1 can represent the chemical compositions of the TM and TH grains of the groups A, B, and C, respectively. Equilibrium temperatures are probably similar within each group.

Note that the present estimates are semi-quantitative evaluations. This is because the present EPMA analytical results have uncertainties of ~ 1 and 2 mol% when the content of ulvöspinel and ilmenite in the TM and TH solid solutions are being calculated, respectively (Section 3). The geothermometer is also designed for stoichiometric pairs of TM and TH (Ghiorso, 1997). As the present TM and TH phases contain some minor substitutions, real equilibrium temperatures may slightly differ from the present estimates. However, the present results indicate that the equilibrium temperature of the group B samples is $\sim 300^\circ\text{C}$ lower than the Curie temperature of the magnetite. This gap seems too large to be caused by the extent of these uncertainties. The uncertainties of 2 mol% in ilmenite content in the TH solid solutions result in errors of up to $\sim 90^\circ\text{C}$ in the present equilibrium temperature estimates (error bars in Fig. 6).

6. Plausibility of Lamellae Nucleation at Low Temperature

Although the geothermometer suggests equilibration at $\sim 300^\circ\text{C}$ for the TM grains of group B samples, it seems to take long time to equilibrate at such low temperature. It is important to consider whether or not these equilibrations (nucleation of ilmenite lamellae) can be achieved be-

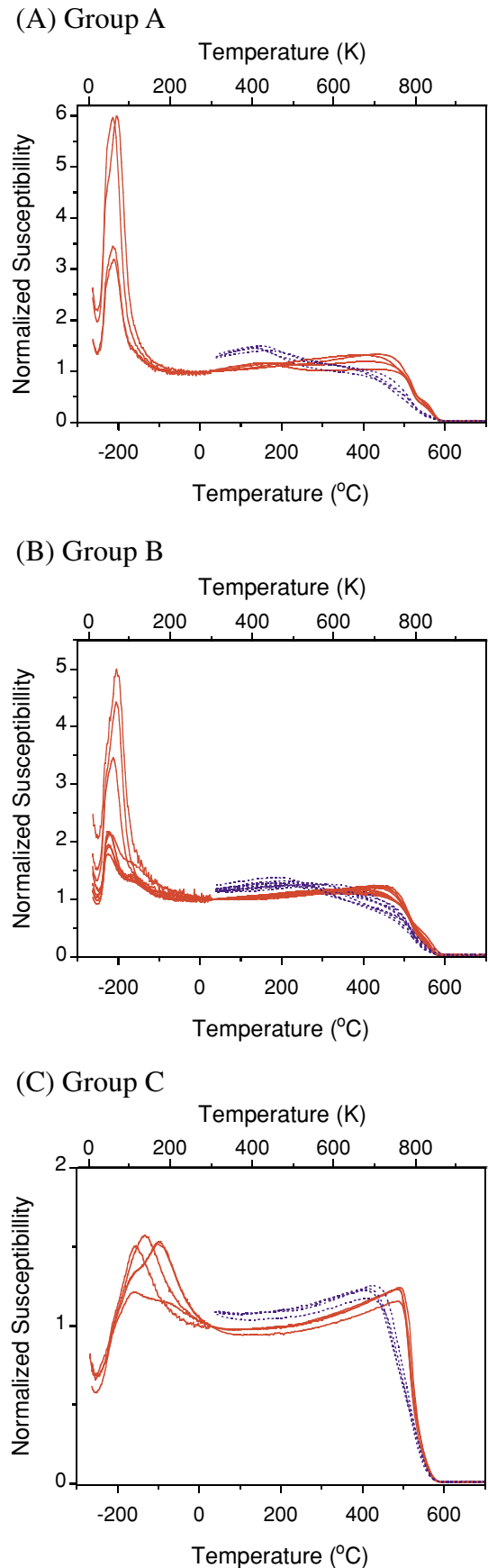


Fig. 7. Temperature-dependent magnetic susceptibility curves for each group. Four, nine and four samples were measured for the groups A, B and C, respectively. Solid (dashed) lines represent heating (cooling) curves.

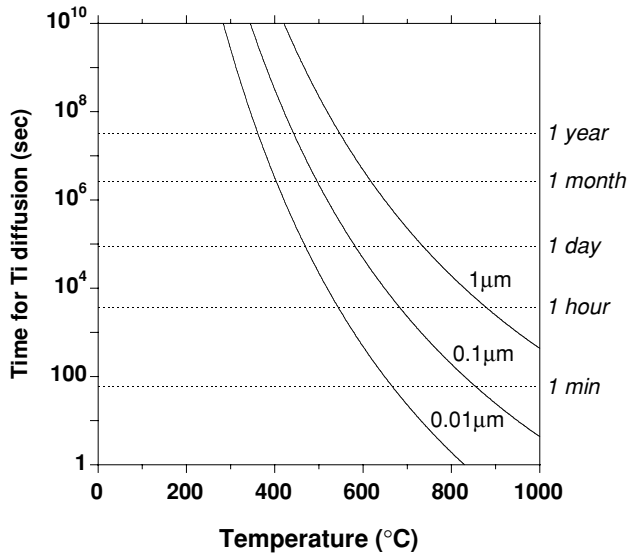


Fig. 8. Temperature dependence of time required for Fe-Ti interdiffusion in magnetite and titanomagnetite. Solid lines show time for 1, 0.1, and 0.01 μm diffusions based on the diffusion coefficient of D ($10^{-3} \text{ m}^2/\text{s}$) = $3.85 \exp(-2.23 \text{ eV}/kT)$ by Freer and Hauptman (1978).

fore a complete cooldown of the lava. According to Freer and Hauptman (1978), Fe-Ti interdiffusion in magnetite and titanomagnetite is dominated by a diffusion of Ti, with a diffusion coefficient of D ($10^{-3} \text{ m}^2/\text{s}$) = $3.85 \exp(-2.23 \text{ eV}/kT)$ for TM0 single crystal and TM20 powder. To the author's knowledge, there is no other experimental data for the Fe-Ti interdiffusion in the TM system. Similar to Freer and Hauptman's dimension analysis, if diffusion time t is estimated from $t = a^2/4D$ (a : diffusion distance) for $a = 0.01, 0.1,$ and $1 \mu\text{m}$, the results are as shown in Fig. 8. These results are thought to be reasonable when the present lamella nucleation state is being considered because the widths of the observed lamellar TH phase in B-6 are in the order of $0.1\text{--}1 \mu\text{m}$ (Fig. 2). The lamella width of $\sim 0.01 \mu\text{m}$ also seems to be a possible scenario since the high-temperature oxidation reduces an effective grain size of relic TM phase, resulting in a lower diffusion distance for subsequent oxidation (Venezky and Rutherford, 1999). There may be a number of such fine ilmenite lamellae in the TM grains of the group B samples, however the magnification at which the EPMA observations were carried out was not high enough to determine their existence.

The time scale of the lava cooling limits the time available for Fe-Ti interdiffusion. The Kilauea 1960 lava probably takes a few months to completely release heat. According to the observations by Richter *et al.* (1970), this lava was formed by a frank eruption of the Kilauea's east rift zone that began on January 14, 1960 and continued for 37 days. The one-dimensional heat equation gives a consistent characteristic time scale of $\sim 10^7 \text{ s}$ (a few months) for a 5-m-sized body. Alternatively, the Kilauea 1960 lava may possibly retain heat for a few years because direct measurements of temperature in the Alae (AD1963) and Makaopuhi (AD1965) lava lakes, Kilauea, revealed that temperatures at $\sim 5 \text{ m}$ in depth from their surfaces were above 500°C at least for 2 years (Wright *et al.*, 1976). Therefore, it is possible

to consider that the Kilauea 1960 lava at Yamamoto *et al.*'s (2003) sampling point ($\sim 5 \text{ m}$ thickness) retained a hot interior (above $400\text{--}500^\circ\text{C}$) for a few months, or possibly even a few years. In this case, the lamella nucleation ($\sim 0.01 \mu\text{m}$) could have occurred at temperatures above $\sim 350^\circ\text{C}$ (Fig. 8).

However, it should be noted that the present discussions of the time scale of the Fe-Ti interdiffusion is based on semi-quantitative evaluations, because the diffusion coefficients for the present TM grains probably differ from those of Freer and Hauptman (1978). The coefficients of these two researchers were determined from interdiffusion experiments at high temperatures (above 600°C), while those of the present evaluation are based on their extrapolations to low temperatures. In addition, the chemical compositions of the TM systems are not exactly the same between the experiments by Freer and Hauptman (1978) and those used in the present investigation. It might be possible that lamella nucleation could have occurred below 350°C . One of the probable scenarios for this would be a pre-condition of relatively high oxygen fugacity, which would enable a faster Ti diffusion than the above estimations given that the Ti diffusion coefficient in the TM system is roughly proportional to the oxygen fugacity (Freer and Hauptman, 1978). Although Fig. 6 suggests concentrated equilibrium temperatures of $\sim 300^\circ\text{C}$ for B-6, which is clearly lower than 350°C , this may possibly be an achievable condition.

7. TCRM/TRM Ratio and Overestimation of Paleointensity

If ilmenite lamellae were nucleated at a low temperature, sub-divided TM domains could acquire TCRM. Although accurate theoretical modeling of just such a TCRM acquisition process seems to be difficult, it may occur as follows.

(1) Original homogeneous Ti-rich TM grains (approx. TM60) gradually deplete Ti by lamellae nucleation, resulting in gentle sub-divisions of TM grains (e.g. Fig. 1, A5 and 1, A9).

(2) The divided domains are gradually enriched in Fe. With these developments in the ilmenite lamellae, Fe-enriched regions are increasing their relative volumes and their compositions are approaching approximately TM05 (e.g. Fig. 2, A9). These reactions could occur at temperatures as low as $\sim 350^\circ\text{C}$ (Section 6).

(3) Since the reaction temperature ($\sim 350^\circ\text{C}$) is higher than the Curie temperature of TM60 ($\sim 145^\circ\text{C}$) but lower than that of TM05 ($\sim 545^\circ\text{C}$), this process could be interpreted as one in which the new magnetic phase (TM05: divided TM domains) is emerging from the paramagnetic phase (TM60: host TM grain) with an increase in its relative volume. This seems to be analogous to a grain-growth of new magnetic mineral below its Curie temperature.

Although this is not a unique scenario of possible TCRM acquisition, if we did assume that it could occur, a TCRM/TRM ratio for an assemblage of identical TM domains would be roughly estimated by the grain-growth CRM model of McClelland (1996). In this model, CRM and TRM for an identical assemblage of grains with volume v_{max} are expressed as follows.

$$\text{CRM} = v_{\text{max}} J_{s0} \frac{v_b H J_s (T_{\text{crm}})}{3kT_{\text{crm}}},$$

$$\text{TRM} = v_{\max} J_{s0} \frac{v_{\max} H J_s(T_b)}{3kT_b},$$

where T_{crm} is the temperature of the CRM reaction, T_b is the blocking temperature, v_b is the blocking volume, v_{\max} is the final grain volume, $J_s(T)$ and J_{s0} are spontaneous magnetization at temperature T and room temperature, H is the ambient field, and k is the Boltzmann constant. Note that this model is developed for the case of constant T_{crm} and a constant new phase composition. In the case of TCRM acquisition, the grain-growth is considered to accompany simultaneous temperature decrease as well as a gradual change in new phase composition.

A ratio of CRM/TRM for the assemblage is given by a following formula.

$$\frac{\text{CRM}}{\text{TRM}} = \frac{v_b}{v_{\max}} \cdot \frac{J_s(T_{\text{crm}})}{J_s(T_b)} \cdot \frac{T_b}{T_{\text{crm}}} \quad (1)$$

In the present scenario, T_{crm} is lower than T_b ($T_{\text{crm}} < T_b$) and $J_s(T_{\text{crm}})$ is larger than $J_s(T_b)$ ($J_s(T_{\text{crm}}) > J_s(T_b)$). Thus, the TCRM/TRM ratio for the assemblage of identical TM domains is controlled by two variables of v_b and v_{\max} . These variables seem to vary with degrees of high-temperature oxidation. If we consider TM grains of C3–C4 oxidation (e.g. Fig. 2, A9), the TM domains are very tiny so that it might be possible to assume $v_b \sim v_{\max}$. In this case, TCRM is always larger than TRM. An example calculation of the TCRM/TRM ratios for a TM0 SD assemblage is listed in Table 5 using the assumption of $v_b \sim v_{\max}$ and $J_s(T)$ data by McClelland (1996). The calculations were made for the case of $T_{\text{crm}} = 350$ and 400°C . This table indicates that the TCRM/TRM ratio ranges between 1.19 and 1.72 for the T_b interval of 400 – 480°C . Since the vicinity T_b portion is often adopted for the Thellier paleointensity calculation, one may expect 20–70% of overestimation in paleointensities from samples containing TM grains of C3–C4 oxidation. This extent of overestimation is comparable to that observed in the group B specimens of Yamamoto *et al.* (2003) (including B-6, ~55% overestimation). Although Smirnov and Tarduno (2005) recently suggested a low-field Thellier paleointensity bias due to TCRM acquisitions, this was derived from an assumption that characteristic relaxation times for TRM and TCRM were comparable. This is different from the present assumption.

8. Conclusion

I have estimated equilibrium temperatures of titanomagnetite grains, which are involved in samples previously subjected to Thellier paleointensity determinations by Yamamoto *et al.* (2003). The temperatures are evaluated by the Fe-Ti oxide geothermometer of Ghiorso (1997). The results show that the specimens from the groups A and C (relatively ideal Thellier paleointensities) have clustered equilibrium temperatures of about 800 – 900 and 700 – 800°C , while two swarmed temperatures around 300 and 700°C are observed for the specimen from the group B (high Thellier paleointensities). Although they are semi-quantitative estimates, considering time scales of Fe-Ti interdiffusion and lava cooling, the last specimen could acquire the TCRM during its formation. For such specimens, simple calculation predicts that TCRM/TRM ratios could result in

Table 5. TCRM/TRM ratios for $T_{\text{crm}} = 350^\circ\text{C}$ and 400°C estimated for a TM0 SD assemblage using the assumption of $v_b \sim v_{\max}$ and $J_s(T)$ data by McClelland (1996). T_{crm} , temperature of CRM reaction; T_b , blocking temperature; v_b , blocking volume; v_{\max} , final grain volume; $J_s(T)$, spontaneous magnetization at temperature T .

T_b ($^\circ\text{C}$)	$J_s(T)$	$J_s(T_{\text{crm}})/J_s(T_b)$	T_b/T_{crm}	TCRM/TRM
$T_{\text{crm}} = 350^\circ\text{C}$				
350	0.712	1.000	1.000	1.000
400	0.646	1.102	1.080	1.191
450	0.565	1.260	1.161	1.462
480	0.500	1.424	1.209	1.721
530	0.341	2.088	1.289	2.691
555	0.190	3.747	1.329	4.980
565	0.080	8.900	1.345	11.971
$T_{\text{crm}} = 400^\circ\text{C}$				
400	0.646	1.000	1.000	1.000
450	0.565	1.143	1.074	1.228
480	0.500	1.292	1.119	1.446
530	0.341	1.894	1.193	2.260
555	0.190	3.400	1.230	4.183
565	0.080	8.075	1.245	10.055

1.19–1.72 for the blocking temperature range of 400 – 480°C assuming the grain-growth model by McClelland (1996). This portion is often adopted for the Thellier paleointensity calculation, and the extent of the overestimation (20–70%) is comparable to the observations in Yamamoto *et al.* (2003). In TM grains of C3–C4 oxidation, one can expect coexisting Ti-poor TM domains (~TM05) and Ti-rich TH lamellae (~ILM95). Equilibrium temperatures of these grains are generally far below Curie temperatures of the corresponding TM domains, as suggested from Fig. 6. If the TM grains associated with well-developed fine ilmenite lamellae and exsolved TM domains were very tiny, they satisfied the condition of $v_b \sim v_{\max}$. We would pay attention to these grains, since they might be potential sources of the overestimation of Thellier paleointensities up to a few tens of percent.

Acknowledgments. I am very grateful to Shingo Takeuchi for the thorough assistance of the EPMA operation and many helpful comments concerning the time scales of the Fe-Ti interdiffusion and the lava cooling. I also appreciate an insightful comment of Masaru Kono at the 2004 JEPS meeting which shed light on the consideration of the lamella nucleation. Takeshi Saito, Koji Uno and Kuniyuki Furukawa are acknowledged for valuable discussions on observations of the Fe-Ti oxides. I thank Toshitsugu Yamazaki and Hirokuni Oda for critical reading of the manuscript, and Yongjae Yu, Alexei V. Smirnov and Hidefumi Tanaka for constructive reviews. Y. Yamamoto is supported by Research Fellowships of the Japan Society for the Promotion of Science for Young Scientists.

References

- Anderson, A. T., Oxidation of the La Blanche Lake titaniferous magnetite deposit, *Quebec J. Geol.*, **76**, 528–547, 1968.
- Biggin, A. J. and D. N. Thomas, Analysis of long-term variations in the geomagnetic poloidal field intensity and evaluation of their relationship with global geodynamics, *Geophys. J. Int.*, **152**, 392–415, 2003.
- Buddington, A. F. and D. H. Lindsley, Iron-titanium oxide minerals and synthetic equivalents, *J. Petrol.*, **5**, 310–357, 1964.
- Calvo, M., M. Prevot, M. Perrin, and J. Riisager, Investigating the reasons for the failure of paleointensity experiments: a study on historic lava flows from Mt. Etna (Italy), *Geophys. J. Int.*, **149**, 44–63, 2002.
- Carmichael, I. S. E., The iron-titanium oxides of silic volcanic rocks and

- their associated ferromagnesian silicates, *Contrib. Mineral. Petrol.*, **14**, 36–64, 1967.
- Chauvin, A., P. Roperch, and S. Levi, Reliability of geomagnetic paleointensity data: the effects of the NRM fraction and concave-up behavior on paleointensity determinations by the Thellier method, *Phys. Earth Planet. Int.*, **150**, 265–286, 2005.
- Coe, R. S., Paleointensities of the Earth's magnetic field determined from Tertiary and Quaternary rocks, *J. Geophys. Res.*, **72**, 3247–3262, 1967.
- Dodson, M. H. and E. McClelland, Magnetic blocking temperatures of single-domain grains during slow cooling, *J. Geophys. Res.*, **85**, 2625–2637, 1980.
- Dunlop, D. J. and Ö. Özdemir, *Rock Magnetism: Fundamentals and frontiers*, Cambridge University Press, 573 pp, 1997.
- Fox, J. M. W. and M. J. Aitkin, Cooling-rate dependence of thermoremanent magnetization, *Nature*, **283**, 462–463, 1980.
- Freer, R. and Z. Hauptman, An experimental study of magnetite-titanomagnetite interdiffusion, *Phys. Earth Planet. Int.*, **16**, 223–231, 1978.
- Ghiorso, M. S., Thermodynamic analysis of the effect of magnetic ordering on miscibility gaps in the FeTi cubic and rhombohedral oxide minerals and the FeTi oxide geothermometer, *Phys. Chem. Minerals*, **25**, 28–38, 1997.
- Ghiorso, M. S. and R. O. Sack, Fe-Ti oxide geothermometry: thermodynamic formulation and the estimation of intensive variables in silicic magmas, *Contrib. Mineral. Petrol.*, **108**, 485–510, 1991.
- Grommé, C. S., T. L. Wright, and D. L. Peck, Magnetic properties and oxidation of iron-titanium oxide minerals in Alae and Makaopuhi lava lakes, Hawaii, *J. Geophys. Res.*, **74**, 5277–5293, 1969.
- Haggerty, S. E., Oxide textures—a mini-atlas, Oxide Minerals: petrologic and magnetic significance, *Reviews in Mineralogy*, **25**, Mineralogical Society of America, 129–219, 1991.
- Hill, M. J. and J. Shaw, Magnetic field intensity study of the 1960 Kilauea lava flow, Hawaii, using the microwave paleointensity technique, *Geophys. J. Int.*, **142**, 487–504, 2000.
- Ishikawa, Y. and S. Akimoto, Magnetic properties of the FeTiO₃-Fe₂O₃ solid solution series, *J. Phys. Soc. Jpn.*, **12**, 1083–1098, 1957.
- Ishikawa, Y., N. Saito, M. Arai, Y. Watanabe, and H. Takei, A new oxide spin glass system of (1-x) FeTiO₃-x Fe₂O₃. I. Magnetic properties, *J. Phys. Soc. Jpn.*, **54**, 312–325, 1985.
- Kellogg, K., E. E. Larson, and D. E. Watson, Thermochemical remanent magnetization and thermal remanent magnetization: comparison in a basalt, *Science*, **170**, 628–630, 1970.
- Kosterov, A. A. and M. Prevôt, Possible mechanisms causing failure of Thellier paleointensity experiments in some basalts, *Geophys. J. Int.*, **134**, 554–572, 1998.
- Lepage, L. D., ILMAT: an EXCEL worksheet for ilmenite-magnetite geothermometry and geobarometry, *Comput. Geosci.*, **29**, 673–678, 2003.
- Levi, S., The effect of magnetite particle size on paleointensity determinations of the geomagnetic field, *Phys. Earth Planet. Int.*, **13**, 245–259, 1977.
- Mankinen, E. A. and D. E. Champion, Broad trends in geomagnetic paleointensity on Hawaii during Holocene time, *J. Geophys. Res.*, **101**, 21995–22013, 1993.
- McClelland, E., Theory of CRM acquired by grain growth and its implications for TRM discrimination and paleointensity determination in igneous rocks, *Geophys. J. Int.*, **126**, 271–280, 1996.
- Mochizuki, N., H. Tsunakawa, Y. Oishi, S. Wakai, K. Wakabayashi, and Y. Yamamoto, Palaeointensity study of the Oshima 1986 lava in Japan: implications for the reliability of the Thellier and LTD-DHT Shaw methods, *Phys. Earth Planet. Int.*, **146**, 395–416, 2004.
- Nagata, T., Magnetic properties of ferrimagnetic minerals of Fe-Ti-O system, in: Proc. Benedum Earth Magnetism Symp., pp. 69–86, 1962.
- Oishi, Y., H. Tsunakawa, N. Mochizuki, Y. Yamamoto, K. Wakabayashi, and H. Shibuya, Validity of the LTD-DHT Shaw and Thellier paleointensity methods: a case study of the Kilauea 1970 lava, *Phys. Earth Planet. Int.*, **149**, 243–257, 2005.
- Richter, D. H., J. P. Eaton, K. J. Murata, W. U. Ault, and H. L. Krivoy, Chronological narrative of the 1959–1960 eruption of Kilauea volcano, Hawaii, US Geol. Surv. Professional Paper 537-E, E1–E73, 1970.
- Smirnov, A. V. and J. A. Tarduno, Thermochemical remanent magnetization in Precambrian rocks: Are we sure the geomagnetic field was weak?, *J. Geophys. Res.*, **110**, B06103, doi:10.1029/2004JB003445, 2005.
- Stormer, J. C., The effects of recalculation on estimates of temperature and oxygen fugacity from analyses of multicomponent iron-titanium oxides, *Am. Mineral.*, **68**, 1983.
- Tauxe, L., Long term trends in paleointensity: The contribution of DSDP/ODP submarine basaltic glass collections, *Phys. Earth Planet. Int.*, 2006 (in press).
- Thellier, E. and O. Thellier, Sur l'intensité du champ magnétique terrestre dans le passé historique et géologique, *Ann. Geophys.*, **15**, 285–376, 1959.
- Valet, J. P., Time variations in geomagnetic intensity, *Rev. Geophys.*, **41**, 1004 doi:10.1029/2001RG000104, 2003.
- Venezky, D. Y. and M. J. Rutherford, Petrology and Fe-Ti oxide re-equilibration of the 1991 Mount Unzen mixed magma, *J. Volcanol. Geotherm. Res.*, **89**, 213–230, 1999.
- Verwey, E. J. W., Electronic conduction of magnetite (Fe₃O₄) and its transition point at low temperature, *Nature*, **144**, 327–328, 1939.
- Wright, T. L., D. L. Peck, and H. R. Shaw, Kilauea lava lakes: natural laboratories for study of cooling, crystallization and differentiation of basaltic magma, in *The Geophysics of the Pacific Ocean Basin and its Margin*, Am. Geophys. Monogr., **19**, 375–392, 1976.
- Xu, S. and D. J. Dunlop, Thellier paleointensity theory and experiments for multidomain grains, *J. Geophys. Res.*, **109**, B07103 doi:10.1029/2004JB003024, 2004.
- Yamamoto, Y., H. Tsunakawa, and H. Shibuya, Paleointensity study of the Hawaiian 1960 lava: Implications for possible causes of erroneously high intensities, *Geophys. J. Int.*, **153**, 263–276, 2003.
- Yu, Y. and L. Tauxe, Testing the IZZI protocol of geomagnetic field intensity determination, *Geochem. Geophys. Geosyst.*, **6**, Q05H17, doi:10.1029/2004GC000840, 2005.